AIMS Energy

http://www.aimspress.com/journal/energy

AIMS Energy, 6(5): 735–763.
DOI: 10.3934/energy.2018.5.735
Received: 26 June 2018
Accepted: 06 September 2018
Published: 19 September 2018

Review

On circuital topologies and reconfiguration strategies for PV systems in partial shading conditions: A review

Antonino Laudani, Gabriele Maria Lozito*, Valentina Lucaferri, Martina Radicioni and Francesco Riganti Fulginei

Department of Engineering, Roma Tre University, Via Vito Volterra 62, Rome, Italy

* **Correspondence:** Email: gabrielemaria.lozito@uniroma3.it.

Abstract: Photovoltaic (PV) power generation is heavily influenced by mismatching conditions, mainly caused by partial or full shading of an array portion. Such a non-uniform irradiation can lead to severe reductions in the power produced; some techniques, such as array reconfiguration or micro-converters and microinverters technology are aimed at retrieving this power together with the use of Maximum Power Point (MPP) tracker algorithms, while others tend to mitigate the effects that power losses have on the PV system, i.e. overheating and aging. Solutions based on the use of bypass diodes and their re-adapted forms belong to this latter case. The complexity of the problem has shown the need of analyzing the role played by each one of the mentioned aspects; the focus of this paper is to give the reader a detailed review of the main solutions to PV arrays shading present in literature.

Keywords: shading; photovoltaic; reconfiguration; bypass; MPPT; power; array

1. Introduction

Among the most important issues concerning PV power generation the question of mismatching is found. A mismatch condition can be determined by either different properties existing among interconnected cells or modules or differences in the operating conditions; this latter case mainly refers to non-uniform irradiation of the module or array [1, 2].

As a matter of fact, one of the main problems related to photovoltaic panels operation is the issue of partial or full shading, hereafter respectively pointed out as PS and FS. As a result of shading, the phenomenon of hot spotting occurs consisting in the overheating of a portion of a module or an array due to differences in the level of irradiance [3–5]: it is evident that a key point in the evaluation of a shading condition is an accurate measurement of such quantity. Several studies exist in literature aimed at fast and precise estimation of the irradiance level, but such measurements, unlike temperature ones, are generally difficult and expensive. In [6] the authors propose two FPGA based

circuital architectures for real-time monitoring of the solar irradiance of a whole PV plant, provided simple measurements coming from several low-cost circuits distributed in different points of the plant. [7] describes an analytical approach based on the reduced form of the single diode model providing a low-cost solar irradiance sensing. Another problem concerning shading is represented by power losses [8]. If we consider a PV panel, its structure consists of groups of series-connected cells, each of which acts as a current source. If a cell gets shaded its current decreases and such a cell becomes reverse biased and begins acting as a load. As a consequence, the shaded cell dissipates power, thus reducing the amount of power delivered to the load.

Among the most widely used solutions to retrieve the power lost, reconfiguration techniques should be mentioned [9,10]. Reconfiguring a PV array means rearranging its modules in order to achieve a new topology providing higher power with respect to the initial arrangement. Lots of studies concerning this issue are present in literature, proposing both regular and irregular configurations [11–14].

An important side effect of dissipation across the solar panel is the overheating that may facilitate the aging of the panel [15] and, eventually, seriously damage it. In order to provide a real-time tool to detect the state of a PV system, in [16] a method has been developed for on-line evaluation of the progressive degradation of PV devices.

The insertion of bypass diodes in ways that will be discussed in the following sections prevents the shaded cell or module from operating with negative voltages; however, this solution severely alters the P-V characteristic of PV arrays [13, 17], giving rise to multiple Local Maximal Power point (LMPP) that make the detection of the Global Maximum Power point (GMPP) difficult. Hence there is a real need of reliable tools able to isolate the GMPP. Maximum Power Point Tracking (MPPT) algorythms are generally embedded in the microconverter or microinverter stage and they are getting always faster and more precise [18–24]. Partial shading is one of the causes of faults in any components (modules, cabling, converters and inverters) of photovoltaic systems. Since the external operating conditions, such as bad weather conditions, ultraviolet radiation or corrosion, can seriously influence the efficiency, PV modules lifetime, total energy yield and security of the entire PV plant, fault detection and diagnosis of PV system are very important to ensure reliability and to protect the components from damage.

All the mentioned methods to face the problem of shading of PV systems are reviewed in this paper, that is organized as follows: Section 2 illustrates the most widely used circuital models for the simulation of PV cells and some methods aimed at characterizing any PV array configuration. Section 3 presents traditional and innovative reconfiguration techniques while Section 4 analyzes converter-based solutions; the standard practice of the insertion of bypass diodes and some new strategies exploiting their advantages are described in Section 5. Several faults and different detection and diagnosis methods are analyzed in Section 6 and, finally, in Section 7, follow the conclusions.

2. Modeling PV modules and arrays

Among the mathematical models describing the electrical behavior of a module, the most suitable are the One Diode and the Two Diodes models. According to the first one, shown in 1, the current I generated by the module is function of the photogenerated current Iph, which is function of irradiance, temperature and number of PV cells connected in series. The electrical behavior is described by the following equations:

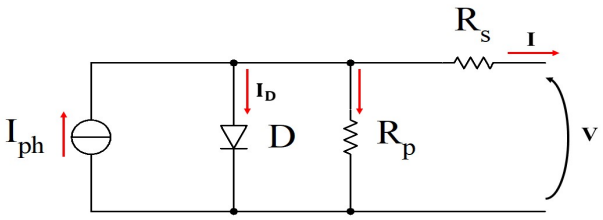

Figure 1. One Diode Model.

$$I = I_{ph} - I_D - \frac{V + IR_S N_{cell}}{R_P N_{cell}} \tag{1}$$

$$I_{ph} = I_{ph(STC)} + K(T - T_{STC}))\frac{G}{G_{STC}} \tag{2}$$

$$I_D = I_0 exp(\frac{V + IR_S N_{cell}}{A(\frac{KT}{q})N_{cell}}) \tag{3}$$

where the parameters represent:

STC: Standard Reference Conditions.
$I_{ph(STC)}$: photo current at STC [A].
$T_{(STC)}$: temperature at STC [K].
T: PV cell temperature[K].
$G_{(STC)}$: irradiance at STC [$\frac{W}{m^2}$].
G: solar irradiance [$\frac{W}{m^2}$].
K: temperature short circuit coefficient.
I_0: reverse saturation current.
q: electron charge (1.602 x 10^{-9} C).
k: Boltzmann constant (1.38 x 10^{-23} $\frac{J}{K}$).
A: diode ideality constant.
R_S: series resistance [Ω].
R_P: parallel resistance [Ω].
N_{cell}: number of series cells.
I_0: diode reverse saturation current.

In many cases PV modules are simulated through a Two Diodes equivalent circuit since, sometimes, it is necessary to introduce a diode to take into account the breakdown caused by high negative voltages [25]. The equivalent circuit is shown in figure 2.

The corresponding equation is slightly different from the one shown for the One Diode model because of the inclusion of the second diode:

$$I = I_{ph} - I_{D1} - I_{D2} - \frac{V + IR_S N_{cell}}{R_P N_{cell}} \tag{4}$$

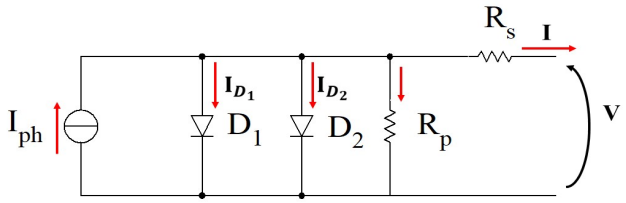

Figure 2. Two Diodes Model.

As evident, in this case there is a different current for each diode:

$$I_{Di=1,2} = I_{0i}exp(\frac{V + IR_S N_{cell}}{A_i(\frac{KT}{q})N_{cell}}) \tag{5}$$

with:
I_{0i}: reverse saturation current of diodes 1 and 2.
A_i: diode ideality factors.

These models are generally used to study the performances of regular array configurations under partial shading conditions, too [26]. As a matter of fact, an issue that recovers a significant role is the need of a tool able to estimate the performance of any PV array configuration; only few models are capable of describing the electrical behavior of an irregular array and under different shading patterns. In [27] such a solution is developed and tested. The PV module is modeled through the One Diode model; therefore, the array is divided into sub-arrays, defined as a set of strings without links with other strings. For each sub-array the parameters of the One Diode model and the connection matrices, indicating the connections existing between strings, are calculated; then, a set of non-linear equations is derived by using nodal analysis. [28] complements this mentioned procedure shown using mesh currents analysis. Finally, an algorithm ensuring global convergence, such as Trust-Region Dogleg, is chosen to solve the system of non- linear equations. The results of the proposed method are compared with those coming from the circuital modeling of the PV array with a commercial software, showing a consistent reduction in the processing time.

3. Reconfiguration techniques

The shading pattern and the array configuration are important factors that influence power output of the array under PS conditions, therefore reconfiguration methods are considered an efficient solution to minimize power losses.

In literature, various reconfiguration schemes have been proposed, they can be classified into two classes: dynamic and static reconfiguration. The first one involves a dynamic reconfiguration of array according to shading pattern by means switches, sensors and controllers. Indeed, the high speed processors and power semiconductors development ensured promising Elecrtrical Array reconfiguration. Moreover, several array reconfiguration algorithm have been investigated to promote shade dispertion, these are based on optimization techniques such as Genetic Algorithm and Particle

Swarm Optimization (PSO) [29, 30]. In [31] an interesting optimization method based on PSO to find the best switch set topology for reconfiguration of PV array has been suggested. Using an objective function, which regards a minimum number of switches and maximum capability to realise different configurations, the optimal topology was reached.

The shortcoming of dynamic reconfiguration relates to the cost of array increased by the inclusion of such sensors and switching as well as the complexity of the hardware and sotware required.

Static reconfigurations employ a fixed interconnection scheme to enhanced the power output under PS. PV modules are physically relocated without altering their electrical connection.

In literature, different interconnection and reconfiguration schemes that follow physical relocation of PV modules without altering electrical connection are available; among these the best known are *Series* (S), *Parallel* (P), *Series-Parallel* (SP), *Total-Cross-Tied* (TCT), *Bridge-Linked* (BL) and *Honey-Combe* (HC), figure 3-4 and Su Do Ku, zig-zag, puzzle shade, respectively.

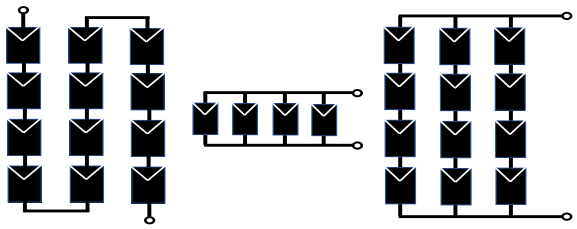

Figure 3. From left to right: Configurations S, P, S-P [25].

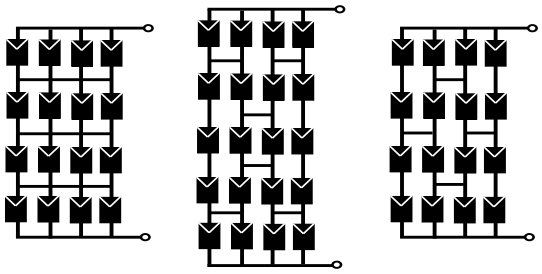

Figure 4. From left to right: Configurations TCT, BL, HC [25].

Series and parallel structures present many drawbacks concerning current and voltage, respectively. In the first one, PV array current is the same as module current, therefore, it is limited by low irradiance level under PS, shaded modules operate in reverse bias condition to generate a short circuit current equal to unshaded PV modules and they dissipate power in form of heat. Although the power produced by the parallel configuration is higher than the one produced by the series one, the higher currents involve greater power losses, so an expensive cabling is required. Therefore, it is preferable an SP scheme, obtained by connecting PV modules in series forming a string to reach higher voltage and then linking the strings in parallel to enhance total current. This scheme is easy to construct, economical and there are not redunant connections, but it has disadvantage such as mismatching losses due to number

of series connections in strings.

The TCT and BL structure are built by introducing connections between string of PV modules in a SP configuration: the first has ties across each row of the junctions whereas the second one has half of these ties. Both allow to decrease the mismatch effects compared to SP configuration. The advantage of BL connection with respect to TCT is the reduction of interconnections, that allow to decrease cable losses; however, the simplicity of pattern makes TCT configuration easier to wire in larger installations.

Finally, HC scheme consists of PV modules interconnected in exagon shape, as such the number of series connections is smaller than other configurations one and mismacth losses are reduced [8].

All six configurations have been compared under different PS and faulty PV conditions through several indicators such as short circuit current, current at maximum power point, open circuit voltage, voltage at maximum power point, series resistance, fill factor and thermal voltage in [32].

In this paper, the choice of the optimal configuration is based on the evaluation of maximum power and lowest power losses, [25], which are computed by the equation:

$$\Delta P_L = \frac{P_M - P_{MPS}}{P_M} \cdot 100 \tag{6}$$

where the maximum power, P_M and P_{MPS}, are calculated under uniform and partially shaded conditions, respectively.

Although these configurations present the same performance under uniform irradiance condition, their behavior changes when a part of the array (a column or a row) is unevenly shaded. In this review, three different shading patterns have been considered:

Condition 1: a row of the array uniformly shaded.

Condition 2: a column unevenly shaded.

Condition 3: different patterns distributed randomly.

The results [25] are shown in figure 5, 6, 7 .

Results show that P configuration is the best one concerning both power losses and output power. Furhermore, it is worth noting that the configuration SP, TCT, BL and HC produce the same results in terms of maximum power and power losses, in the first condition. Aside from P configuration, Figure 6 illustrates TCT arrangement produces the highest power (1,27 kW) and the lowest power losses (14%), while S topology has the worst performances. The results of Condition 3 are similar to those of Condition 2 since the maximum power is provided by TCT configuration (0.67 kW) against 0.49 kW generated by S scheme.

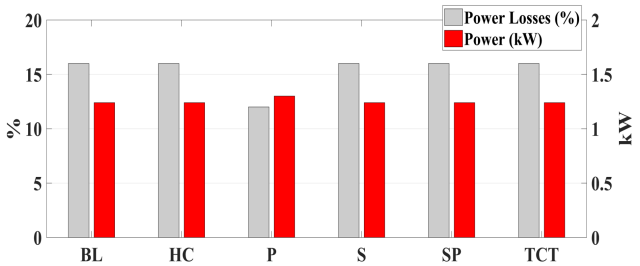

Figure 5. A row of the array uniformly shaded: comparison among regular configurations [25].

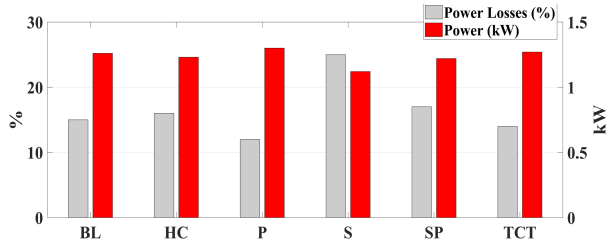

Figure 6. A column unevenly shaded: comparison among regular configurations [25].

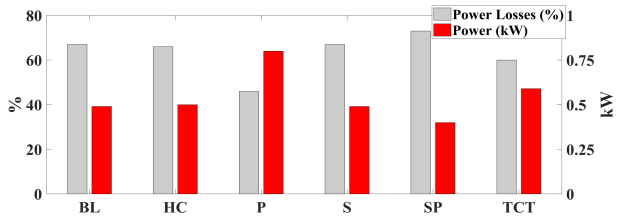

Figure 7. Different patterns distributed randomly: comparison among regular configurations [25].

As already discussed, the TCT interconnection achieves the best results compared to other configurations proposed in [26], but it suffers from certain problems including multiple peaks, excessive length of interconnecting wires leading to increased losses and mismatch losses when the number of shaded panels in a row is higher. This last problem may be dealt by the Su Do Ku puzzle arrangement which allows to reconfigure the panels in the array with the aim of preventing bypass diodes. The reconfiguration involves physical displacement of the panels from their original location to a new location in any row, but within the same column provided by the solution of the puzzle. The electrical connections remain unaltered as in a normal TCT structure. The dispertion of panels by moving the modules to different rows as per Su Do Ku arrangement reduces the probability of shading panels in the same row, therefore an increase of line losses is given by the length of the wire required. In [33] an optimal Su Do Ku pattern to reduce line losses and to increase shading dispersion in a 9x9 PV array is discussed.

Recently, researchers have introduced new arrangements based on maximizing the distance between PV modules by ordering them in different rows and columns without altering electrical interconnections of traditional TCT scheme. In paper [26], new topologies with shifting array arragement have been derived by changing the physical location of PV modules for each PV array. Replacement is necessary to maximize the GMPP and reduces the peaks in PV characteristics, while shifting allows to distribute the shadow pattern on the entire PV array and mitigate its impact. The only drawnback concerns the wasted space, to overcome it extra space is filled up with PV modules

from separate PV sub-array, then *new shift modified TCT*, S-M-TCT configuration is obtained, figure 8. Furhtermore, a blocking diode may be inserted for each PV panel to enhance the efficiency of S-M-TCT arrangement, SMTCT+BL. The insertion of blocking diodes should improve power consumption, if the diodes resistance is not small enough; therefore an alternative arrangement is presented, in which the sub-array of S-M-TCT can be connected in parallel, //S-M-TCT, reducing the shade-effect and the protection diodes power dissipation.

The performance of these three variants have been assessed according to maximum power generated and compared to existing configurations, such as SP and TCT. Again, the performances are evaluated in the scenarios illustrated before, i.e. Condition 1, Condition 2 and Condition 3. The results, shown in figure 9, 10, 11, highlight the advantages of the new arrangements; the three variants yield higher power output under different shading scenarios.

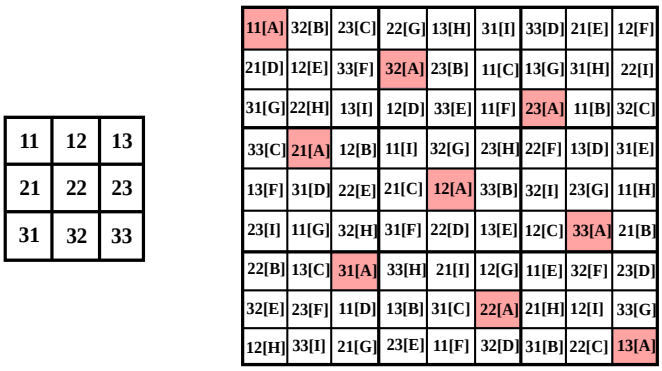

Figure 8. From left to right: TCT arrangement and physical location of S-M-TCT arrangement [26].

To minimize the effects of PS, new zig zag method was proposed in [34]. In another work [35], a new puzzle based reconfiguration scheme is proposed and tested with 5 x 5 PV array. The dominance square method configures the PV modules of convetional TCT interconnection. Thus, row and column wise rearrangement helps to attain uniform current difference with the method.

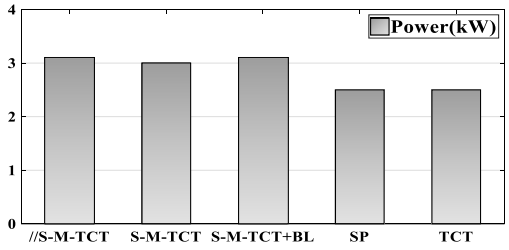

Figure 9. A row of the array uniformly shaded: comparison between regular and irregular configurations [26].

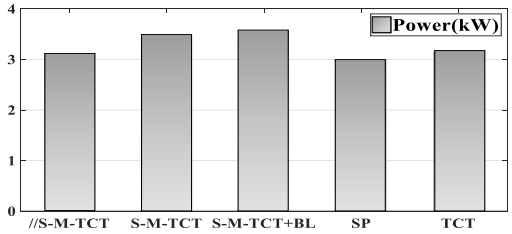

Figure 10. A column unevenly shaded: comparison between regular and irregular configurations [26].

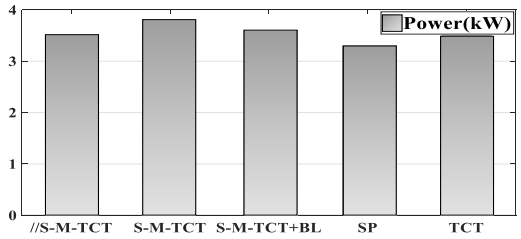

Figure 11. Different patterns distributed randoml: comparison between regular and irregular configurations [26].

4. Converter-based solutions

The need to increase the efficiency of PV plants, despite of possible bad atmospheric conditions, has also produced a relevant development in PV power converters technology; as a matter of fact, innovative topologies have been developed in the last two decades to face the issue of improving PV plants performances and converters have become more and more compact and efficient.

The standard topology of a grid-connected PV system, figure 12, generally consists of the PV module(s) itself, an optional stage including an input filter and a dc-dc converter, the PV inverter and the output filter; eventually, a low-frequency transformer is added at the end. The cited optional stage is responsible for decoupling the operating point of the PV system from the inverter and can increase PV output voltage, provide galvanic isolation for safety reasons and MPP tracking. The main requirements that the new generation of converters has to satisfy include efficiency around 98%, life-time around 25

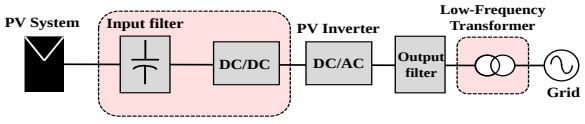

Figure 12. Typical structure of a grid-connected PV system.

years to match that of PV modules, MPPT control and minimal leakage currents. Recently, several solutions have been studied and developed both concerning the dc-dc stage and the dc-ac one. In the following subsections these two parts are analyzed separately.

4.1. Dc-dc Converter topologies

In a typical grid-connected PV system, the dc-dc stage is needed to match the PV output voltage with that of the inverter dc bus. One of the most promising solutions seems to be the use of MIC (Module Integrated Converters): highly efficient dc-dc converters equipped with galvanic isolation that can be integrated in the module. The galvanic isolation ensures reduction of leakage currents towards ground and of harmonics. In paper [36] the advantages of MICs and DPP (Differential Power Processing) Converters are combined in a device able to increase the efficiency of the system. DPP is a technique that delivers part of the power generated by unshaded modules of the array to shaded ones so that every cell of the array has the same operating voltage. A Switched Capacitor Converter (SCC) is proposed allowing to reduce the size of the storage element thanks to the use of capacitors, instead of inductors. Among SCCs, Resonant SCC (RSCC) has been chosen because of its capability of keeping switching losses low and of avoiding current picks during charging and discharging. The presented device consists of a half-bridge and two resonant tanks, carefully designed to be efficient in a wide input voltage range; two MOSFETs act as switches and are activated in a complementary way; one of the tanks, placed between the switches, is responsible for the transfer of power from unshaded to shaded modules. Finally, the scheme ends with a balancing circuit able to provide a doubled output voltage, figure 13. The presented device is able to reach an efficiency of 97.75% and to ensure reduction of power losses up to 20%. These encouraging results partly depend on the single-stage topology of the device presented; as a matter of fact, in a double-stage converter the first stage consists of a boost converter aimed at stepping-up the voltage of the PV module; however, the boost converter is not suitable for heavily shaded patterns and this badly affects the performances of the system. It will be shown that this solution is the best one with respect to others based on buck-boots converters. Among existing solutions, an approach is proposed in [37] consisting of multiple capacitor-inductor diode filters (CLD) stacked on standard buck-boost converters: in this study, the SEPIC (Single Ended Primary Inductor Converter) is considered. In the proposed architecture the number of switches is reduced to one, thus simplifying the circuitry with respect to traditional DPP converters. The device here discussed is referred to as voltage equalizer since its function is the redistribution of the power generated by a PV array to the set of substrings of which is constituted according to their level of shading: this guarantees that all substrings operate at the same voltage. The control circuit supplying the equalization current implements a PWM scheme. The system, figure 14, is, then, equipped with an MPPT converter tracking the MPP of each string by adjusting its input current; the equalization process, also, eliminates the local MPPs and increases the values of the maximum power extracted. Efficiency reaches the value of 87%.

In [38] an innovative approach is presented consisting in a MIC made up of a dc-dc buck-boost converter with galvanic isolation; the system, referred to as PVMIC (Photovoltaic Microcon-verter), is also equipped with an MPP tracker. Since different shading conditions can determine different Vmpps, the PVMIC must have wide voltage range. According to the various operating conditions, the PVMIC has three operation modes: the boost mode provides voltage regulation at low temperatures, the buck one is suitable with PS and high temperatures and the normal mode ensures maximum

efficiency. As an alternative, the converter can be substituted with a quasi-Z-source series resonant dc-dc converter (qZSSRC) [39] characterized by a single switching state, instead of two. This solution allows to reduce the number of components since single-switch topology can be implemented, reducing switching losses. The qZSSRC based solution allows to reach a peak efficiency of 97%.

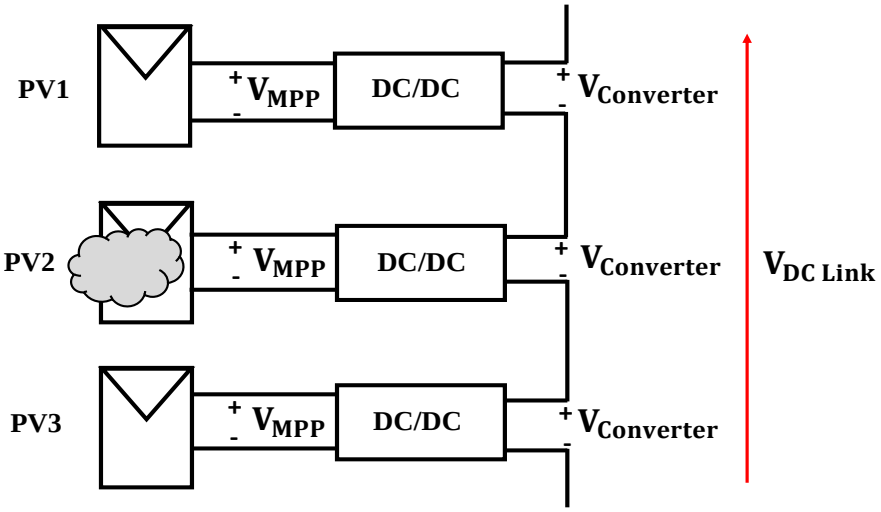

Figure 13. System block diagram of RSCC-based solution [36].

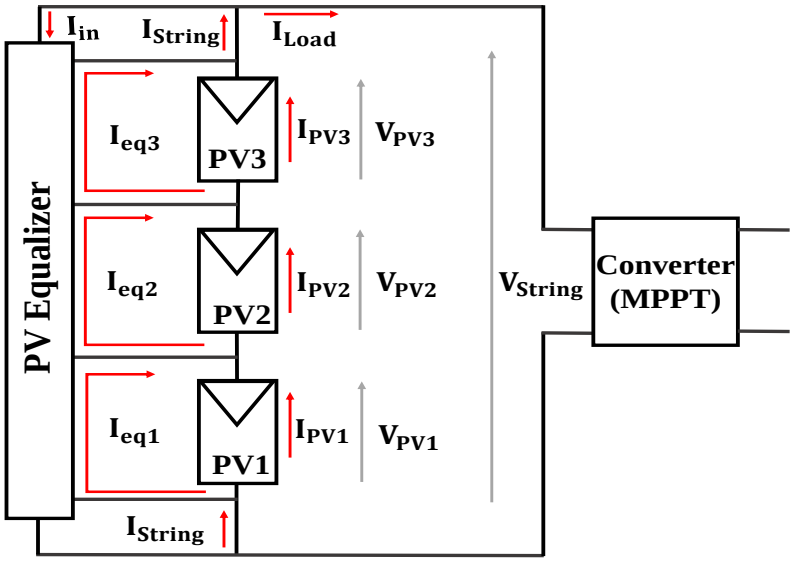

Figure 14. Schematic of PV string with the proposed Voltage Equalizer solution [37].

4.2. Dc-ac Inverter topologies

The inverter configurations can be manifold, but they are generally classified into three main classes. Microinverters are a technology that, in the last years, is spreading in photovoltaic scenario and that is rapidly growing and developing, in particular in low power plants. The pros deriving from the use of microinverter technology are manifold from both a technical and a commercial point of view [40]. A fundamental feature concerning PV installation is the trend to reduce the size of the area intended for the installation itself; as the development in semiconductor technologies has made possible the introduction of the concept of Building Integrated Photovoltaics (BIPV), inverters are getting always smaller, allowing to keep following this trend. This led to the introduction of the afore-mentioned miniaturized inverters (microinverters) that make easier the set-up of power plants. Because of the low-voltage rating of PV modules, these inverters need the afore mentioned dc-dc stage to enhance voltage; their low efficiency is compensated by very efficient MPP tracker systems. Microinverters are suitable for heavily shaded scenarios and, thanks to their compactness, for small plants such as domestic ones. One of the main advantages of microinverters, derives from their configuration. Traditionally, inverters used to follow the centralized configuration, figure 15, in which all the modules constituting the array end in a single dc-ac converter. They are suitable for large-scale plants; this implies that the cabling has to be dimensioned for high dc voltages, causing problems of safety and the need for cooling systems. A blocking diode is in series to each string to provide protection in case of mismatching. Since a single inverter is employed, the MPPT accuracy is the lowest of all other topologies. On the other side, string configuration provides each string with its own inverter; this improves reliability but the issues about cabling still persist. Moreover, if a group of modules is shaded, this affects the whole string. However, with respect to microinverters, string inverters have lower costs per watt and have higher efficiencies, but the MPP tracking stage is less accurate; they are employed for small to medium plants. If we compare string inverters, figure 16, with microinverter configuration, figure 17, it can be noticed that in this latest topology each panel of the string is provided with its own converter. This aspect is fundamental, since allows to free one panel from the other and avoids system-wide failures. In addition to this, many other advantages are worthy of note:

- the dimensions of the system are reduced;
- the mentioned microinverter configuration simplifies the design stage, reducing the costs of installation. Moreover, since each module has its own device there is no need for high voltage dc switches and protection circuitry that is, instead, required for centralized configurations;
- the system is smart and reliable;
- there is no need for bypass diodes (their use will be discussed in the following section);

Nevertheless, some improvements should be carried out in the next generation of inverters; of course, their lifespan could be extended to match the 20–25 years of a PV module and as mentioned in [41] some solutions have already been studied. Then, bringing efficiency beyond 95 % is nowadays a critical point since microinverters are aimed at BIPV use and so, involve low power levels; in addition to this, it has to be noticed that each microinverter has its own circuitry involving additional losses. In [42] DPP is used again, in a two-switch voltage equalizer using an LLC resonant inverter and a voltage multiplier. The elimination of multiple dc-dc converters allowed to reduce the number of switches and, thus, to simplify the circuitry and the equalizer is designed to achieve minimum power consumption when no PS occurs. Peak efficiency is 95%. A highly efficient microinverter

architecture is shown in [41] consisting in a dc-dc flyback converter plus a resonant full-bridge inverter. Among microinverters architectures, the choice has fallen on the flyback one because of its topological simplicity and good performances as far as low power applications is concerned. The system presented in this study guarantees zero voltage drop of the switches during turn-on and turn-off, avoiding power losses. The substitution of a traditional electrolytic capacitor with a film one, finally, ensures extension of the microinverter lifespan. The efficiency of the devices approaches 97.5%. To draw up an accurate quantitative analysis of the two main conversion technologies employed for small and medium plants, i.e. string inverter and microinverter, the authors of paper [43] evaluated the performance of different topologies and shading conditions for both cases. In particular, six scenarios have been analyzed, two string-inverter configurations with no shadow (S_1 and S_2) and four microinverters cases M_1, M_2, M_3 and M_4 respectively with 9.4%, 12%, 0% and 5.4% of shading. Two performance indexes are taken into account to evaluate the performance of the aforementioned technologies: the Performance Ratio (PR), defined as the ratio between energy produced per peak power installed and the radiation received per irradiance of the site and the Efficiency, the ratio between produced energy and irradiation received. As shown below in figure 18, microinverters are confirmed to be the most efficient technology.

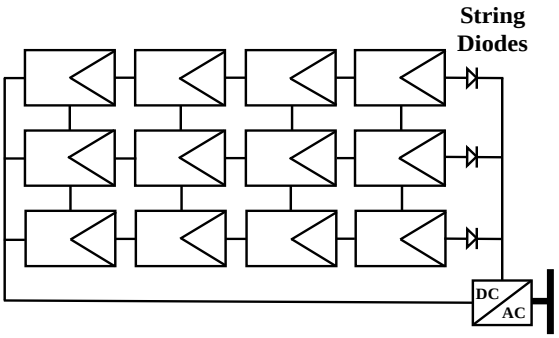

Figure 15. Centralized Inverter Configuration [43].

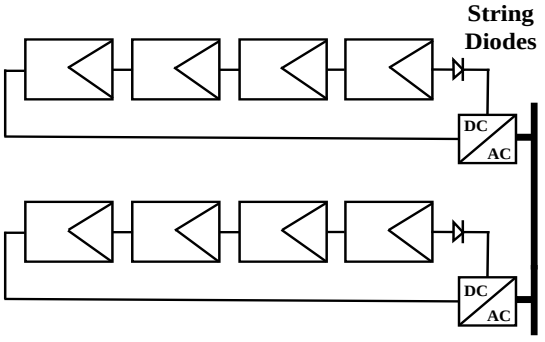

Figure 16. String Inverter Configuration [43].

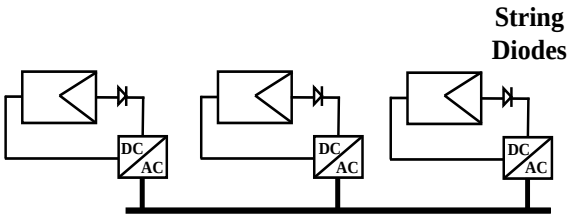

Figure 17. Microinverter Configuration [43].

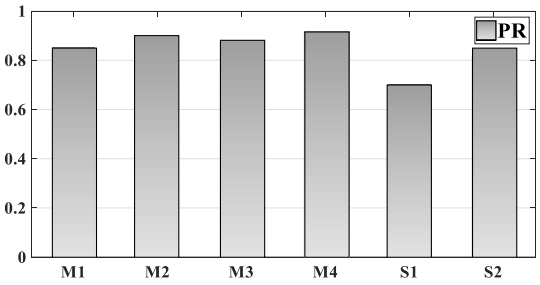

Figure 18. String Inverter vs Microinverter configuration performances [43].

5. Bypass Diodes: traditional and new solutions

As already mentioned, hot spotting is a main problem in PV panels seriously affecting their performances. If we consider a single cell getting shaded it is obvious that its irradiance level is lower with respect to that of the other cells; as a consequence of this, the current produced by the shaded cell is reduced and this affects the whole panel since the other cells are forced to produce higher voltages than can lead the shaded cell to operate in reverse bias mode. In this case, the shaded cell starts acting as a load and a significant part of the power produced by the rest of the panel is dissipated through the failing cell that, as evident, degrades the performances of the whole panel. Moreover, the concentration of such a power in a small area, i.e. the limiting cell, leads to local overheating known as hot spots causing further issues. As a matter of facts, degradation of the encapsulant of the cells, severe damages and aging of the panel can occur as a consequence of high temperatures. Two main parameters are generally evaluated to analyze the state of a shaded panel, namely the breakdown voltage and the shunt resistance; the first one indicates the maximum reverse voltage that can be approached ensuring safe operation of the cell: going beyond this value leads to a sudden increase of the reverse current that may damage the device. Moreover, it is worth noticing that, when overheating occurs, the cell can also go through what is called second breakdown, a phenomenon that can bring the temperature above 400 °C leading serious permanent damages. The shunt resistance, instead, stands for unwanted current paths, again indicating malfunctioning of the cell.

The standard practice aimed at reducing overheating consists of using bypass diodes inserted in parallel to subpanels or subsections, figure 19, portions of the panel of about 20 cells. The maximum reverse voltage of each substring should be maintained low in order to ensure safe operation in reverse

bias condition. As a consequence of shading, the shaded cell or group of cells becomes reverse biased; in this scenario bypass diodes become forward biased and allow to cut-off these failing cells, providing an alternative path to the photogenerated current, figure 20. Despite its wide use, this technique presents some drawbacks, such as the voltage drop across bypass diodes, that introduces further power losses. A solution can be found in the use of devices with a null input resistance, such as the Smart Bypass presented in [44] figure 21. The device is a switch whose central element consists of a single reverse-blocking drain-extended NDMOS (RBNDMOS).

Table 1. Simulation results of P_{MPP} for one shaded cell and for N shaded cells [44].

	Power (W)	
	1 cell	**N cells**
Traditional Diode	42.56	16.84
Smart Diode	43.03	29.24

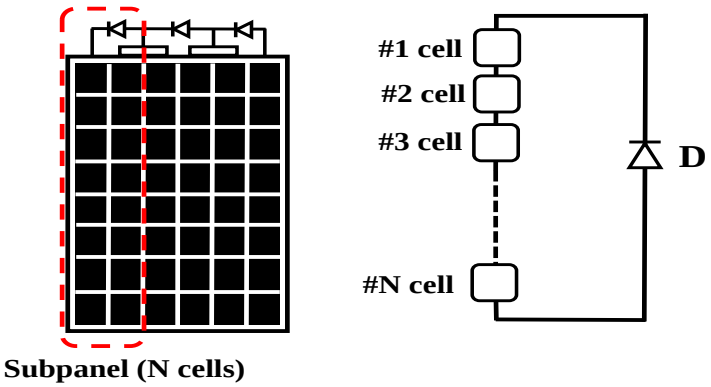

Figure 19. Sketch of a solar panel partitioned into 3 16-cell subpanels, each equipped with a bypass diode.

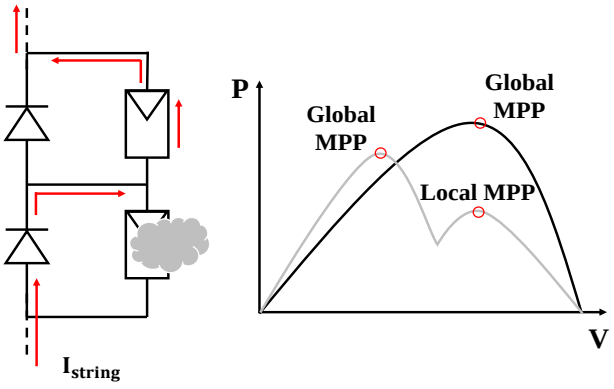

Figure 20. Bypass diodes effects on P-V characteristic.

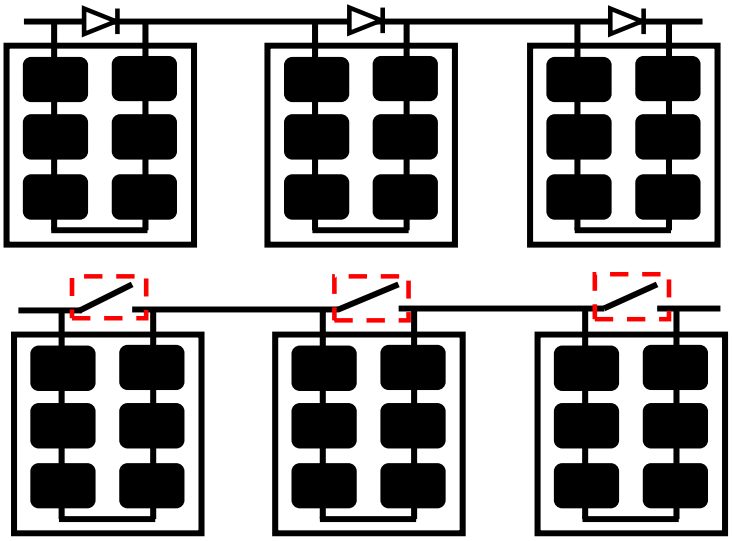

Figure 21. From top to bottom: PV-module model with bypass diodes, with Smart Bypasses [44].

However, traditional bypass diodes can be used in innovative configurations able to exploit their advantages. Another solution based on MOSFETs is shown in [45]; a bypass diode is connected in parallel to each series formed by the subpanel and the power MOSFET. This latest device has the task of lowering the reverse voltage-drop of the shaded cell. When the gate-source voltage of the MOSFET is high, i.e. when the cell is soiled, it acts like a short circuit, current flows and the diode is off; when the cell is shaded the current flowing through the device decreases and the diode is activated: in this case the source-drain voltage arising is subtracted from the reverse voltage of the failing cell, figure 22.

When it is in conduction mode, the bypass can be simulated with a resistor equal to the on-resistance of the NDMOS. Unlike other solutions available in literature, the Smart Bypass just uses one NDMOS, instead of two MOSFETs, and this reduces the size of the switch. The checking of the shadow condition is made by the timer block, based on a capacitor, that generates a signal at regular time intervals, sampling the state of the cell. As far as the prototype is concerned, the switch is designed to handle a load current up to 1A, the input resistance is set to 0.15 Ω and the capacitor of the timer is dimensioned to provide a sampling every 10ms. Power simulations show that the Smart Bypass is effectively able to dissipate much less than the traditional Bypass Diode and, hence, the power delivered to the load is higher, as shown in Table 1. However, traditional bypass diodes can be used in innovative configurations able to exploit their advantages. Another solution based on MOSFETs is shown in [45]; a bypass diode is connected in parallel to each series formed by the subpanel and the power MOSFET. This latest device has the task of lowering the reverse voltage-drop of the shaded cell. When the gate-source voltage of the MOSFET is high, i.e. when the cell is soiled, it acts like a short circuit, current flows and the diode is off; when the cell is shaded the current flowing through the device decreases and the diode is activated: in this case the source-drain voltage arising is subtracted from the reverse voltage of the failing cell, figure 22.

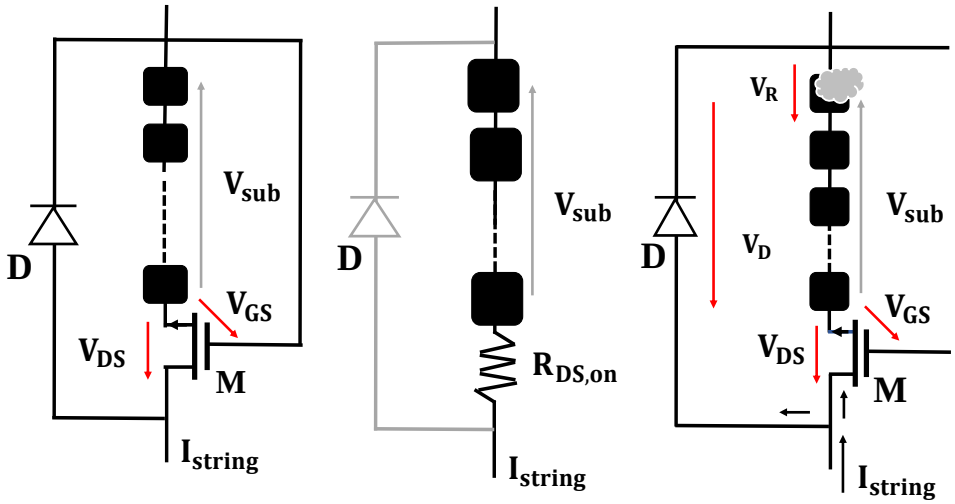

Figure 22. From left to right: Diagram of the bypass strategy proposed in [45]; operation under sunny and shading conditions.

This approach leads to a reduction of power dissipation and is able to reduce overheating also in FS conditions. Moreover, the architecture developed does not require a control logic or power supply. The techniques aforementioned are able to solve the issue of hot spotting, but do not prevent it; as a matter of fact, it is generally thought that the traditional bypass strategy protects the cell from overheating but it an incorrect opinion: all these solutions do not eliminate hot spots that still persist and may lead to the aforementioned drawbacks.

To face this issue other solutions have been developed based on hot spot detection and protection. It has been noticed that when PS occurs the shunt resistance of the circuital model of the substring increases; so, in [46] the measurement of such a quantity is taken as an indication that one or more cells of the substring are shaded.

In [47] two solutions are proposed to mitigate the effect that hot spots can have on solar cells; the first technique consists of connecting to the PV module two MOSFETS, as shown in figure 23: one of the switches is connected in series to the module and is opened, i.e. is in off-mode, when a hot spot condition is detected while the other, in parallel with the string, turns closed, to furnish an alternative path to hot spot currents. The second technique is quite similar, but each string has its own switch, connected in the afore mentioned way: the operating principle is the same as seen before. The two techniques have been applied to a 220 W PV panel and evaluated in terms of temperature reduction and power recovery; the temperature reduction achieved with the first technique is of 5.7 C vs 2.1 C of the second one and, as far as power loss is concerned, with an irradiance level fixed at 840 W/m2, the first technique is, again, the better choice with a value of 3.95 W vs 1.24 W of the second one. Finally, the cost of both techniques is minimal since the cost of the MOSFETS is low.

In [48] bypass diodes are exploited in a particular way since the measurement of their voltage drop is an essential information for the development of an efficient MPPT. As already mentioned, because of the insertion of bypass diodes the detection of the GMPP is difficult, so MPPT algorithms are needed. In the cited paper bypass diodes voltage drop is measured with a voltage sensor and is used to detect

partial shading levels. Then, a lookup table is compiled to associate a shading pattern to the states of bypass diodes, voltage and current of the module are measured and used to perform standard MPPT algorithms (such as Perturb and Observe, P&O). If power oscillations are limited between -5% and +5% the bypass diodes states are used to check whether the operation region is correct; if this is not true voltage is slightly modified to correspond to that of the corresponding region, otherwise P&O is used again to track the MPP continuously. The method has been tested on a 3x3 PV array under various shading conditions and the results show that the energy extracted in a single day is up to 9% higher with respect to traditional MPPT techniques.

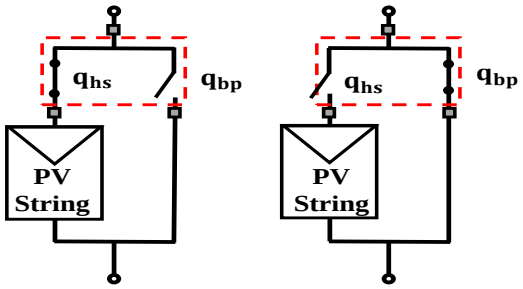

Figure 23. Protection device presented in [47] in normal, left, and hot spot prevention mode, right.

6. Faults and detection and diagnosis methods

Usually, faults in PV modules can be classified into two categories: permanent and temporal. Permanent faults are, for example, delamination, scratches,burnt cells and they can be eliminated by replacing the faulty modules; while, temporal one are caused by partial shading or dirt on PV modules, so substitution is not required.

Monitoring systems are essential to control and to perform fault detection in a photovoltaic plant, so many systems regarding monitoring, diagnosis and power forecasting in photovoltaic system have been recently proposed to detect the malfunctions quickly. They can be divided into five macro-areas [49] :

- electrical methods, based on measurement of electrical parameters executed at array level, single string level and single module level;
- data analysis, that involves machine learning based approaches;
- power forecasting, that concerns the ability to evaluate the producible power of photovoltaic system;
- thermal analysis, based on thermal image capture;
- power converter reliability.

Electrical methods can be used for detecting faulty PV modules such as arc faults, grounding faults and diode faults. They have been discussed in terms of complexity, ability to detect and locate faults in [50]. Among electrical based Fault Detection techniques, an I-V characteristic analysis is proposed in [45]. The novel method is based on simple electrical measurements and involves the first and second derivation of the I-V curve. Recently, a technique based on real time measuring of I-V

characteristic was developed in [51]. It consists in comparing the performances of the faulty module with its accurate model, as has been done in [52–54]. Faulty strings and inverters failures have been investigated in [55] by means of new current and voltage indicators. Whereas, mismatch faults are detected through Arduino-based methods, which exploit the measuring of voltage, temperature and resistance of the modules [56]. Finally, an easy technique able to detect string faults by means of a comparison between measured power and simulated one has been presented in [57]. Machine learning-based approaches require the collection and preprocessing of faulty and healthy data, from an operational PV system, to detect and diagnose eventual faults. Artificial Neural Networks (ANN) and Fuzzy Logic have been used in several works. An ANN has been implemented in [58] to estimate the output PV current and voltage under partial shading conditions. This approach requires as input only solar irradiance, temperature and PV arrays current and voltage, therefore it results easy and cheap. [59] presents a fault detection and diagnosis of a grid connected PV system, based on a probabilistic neural network (PNN). The robustness against noisy measurements was tested under four operating cases, such as healthy system, three modules short circuited in one string, ten modules short-circuited in one string and a string disconnected from the array. Currently, fuzzy logic systems are widely used with grid connected photovoltaic systems. An approach employing a neuro-fuzzy classifier for detection of bypass diodes and blocking diode faults was developed in [60]. [61] proposes a fast and reliable fault detection algorithm concerning fuzzy logic classification system, which allows to detect short circuited PV modules in strings. Standard monitoring approaches are better suited to ensure power loss detection; to achieve an accurate localization of faulty modules a visual inspection or an electrical and thermographic analysis are required. [62] proposes aerial triangulation and terrestrial georeferencing, two different techniques for advanced inspection mapping of PV plants. Faults and infrared thermographic diagnosis have been reviewed in [63]. Among possible faults, those associated with dc-ac power converters are the most dramatic. Although a failure of dc-ac power converters is easy to detect, its occurrence interrupts completely the energy generation. In this field, the challenge is to estimate the residual lifetime of the power modules, related to temperature stresses, in order to prevent failures. In [64] it has been demonstrated that an increase of the level of humidity corresponds to a surge in the leakage current, so a temperature stress occurs.

7. Conclusions

This review paper has analyzed the issue of partial and full shading and its drawbacks as far as power generation by PV plants is concerned. The problem of power losses has been widely discussed and available solutions have been illustrated. The possibility of reconfiguring the PV array providing a new arrangement of the modules able to enhance power production has been described and several solutions have been proposed, concerning both regular and irregular arrangements. As already shown, the better performances are associated to irregular configurations [26] while among regular ones the best is the TCT. The choice of one configuration or another should take into account the particular shading scenario since, among these efficient solutions, there is not an arrangement absolutely better than another. Table 4 provides a detailed scheme indicating the performances of each cited configuration in different scenarios. Moreover, micro-inverter technology has been introduced and its pros and cons have been evaluated. Among traditional solutions, bypass diodes operation has been

explained and some innovative solutions exploiting their advantages have been considered. As previously shown in Table 2 the solution proposed in [44] is a particularly suitable one since exploits an already existing technology, but introduces further improvements. Indeed, the necessity for analytical models to determine the MPP is apparent; as far as this latest aspect is concerned, solutions suitable to be embedded in low-cost devices and providing speed and reliability seem to be the most promising ones [23, 24, 65]. Surely, new solutions could be implemented combining two or more of the most efficient proposals analyzed; some of these could consist in merging the reconfiguration technology with the use of the Smart Bypass or with an efficient MPP algorithm, in order to benefit from both the maximization of power and the reduction of losses. This study would offer an idea of the impact that shading has on the efficiency of a PV system, provide an overview of the state of the art of existing solutions in order to furnish a guideline to researchers working in this field and suggest hints for the development of new solutions.

Table 2. Performances summary of regular and irregular configurations found in literature.

Ref.	Config.	V_{MPP}(V)	I_{MPP}(A)	Generated Power(kW)	Power Losses (%)	n* PV	Notes
[30]		17.18	75.77	1.3	12	6 x 4	A column unevenly shaded
[30]	P	17.18	75.77	1.3	12	6 x 4	A column unevenly shaded
[30]		16.87	71.69	0.49	67	6 x 4	Random shading
[10]		554.2	7.61	4.2	16.5	5 x 5	Shading short and narrow
[10]		137.25	19.96	2.6	47.36	5 x 5	Shading short and wide
[10]	S	133.18	27.42	3.0	40.6	5 x 5	Shading long and narrow
[10]		533.7	3.96	2.0	58	5 x 5	Shading long and wide
[30]		345.07	3.58	1.5	16	6 x 4	A row uniformly shaded
[30]		310.43	3.58	1.12	25	6 x 4	A column unevenly shaded
[30]		310.41	1.58	0.49	67	6 x 4	Random shading
[10]		117.35	31.74	3.7	26.25	5 x 5	Shading short and narrow
[10]		475.4	5.59	2.7	45.75	5 x 5	Shading short and wide
[10]		535.2	5.6	3.6	27.7	5 x 5	Shading long and narrow
[10]		134.04	20.08	2.7	46.9	5 x 5	Shading long and wide
[19]	SP			0.057		2 x 2	Random shading
[30]		86.14	14.35	1.23	16	6 x 4	A row uniformly shaded
[30]		103.44	11.88	1.22	18	6 x 4	A column unevenly shaded
[30]		34.69	11.49	0.4	76	6 x 4	Random shading
[31]				2.5		9 x 9	A row uniformly shaded
[31]				3		9 x 9	A column unevenly shaded
[31]				3.2		9 x 9	Random shading
[33]				0.04		3 x 3	Random shading
[14]				3.6		9 x 9	Shading short and wide
[14]				5.0		9 x 9	Shading long and narrow
[14]				5.3		9 x 9	Shading short and narrow
[19]				0.167		2 x 2	Random shading
[30]	TCT	86.14	14.35	1.23	16	6 x 4	A row uniformly shaded
[30]		103.89	11.88	1.27	13	6 x 4	A column unevenly shaded
[30]		68.95	8.6	0.59	60	6 x 4	Random shading
[31]				2.5		9 x 9	A row uniformly shaded
[31]				3.2		9 x 9	A column unevenly shaded
[31]				3.5		9 x 9	Random shading
[33]				0.05		3 x 3	Random shading
[30]		86.14	14.35	1.23	16	6 x 4	A row uniformly shaded
[30]	BL	104.86	12.02	1.26	15	6 x 4	A column unevenly shaded
[30]		53.56	9.2	0.49	67	6 x 4	Random shading
[33]				0.055		3 x 3	Random shading

Ref.	Config.	V_{MPP}	I_{MPP}	Generated Power(kW)	Power Losses (%)	n* PV	Notes
[10]		137.36	27.61	3.8	24.91	5 x 5	Shading short and narrow
[10]		138.88	20.19	2.8	43.86	5 x 5	Shading short and wide
[10]	HC	135.48	27.76	3.8	25.5	5 x 5	Shading long and narrow
[10]		135.78	20.19	2.7	45.7	5 x 5	Shading long and wide
[30]		86.21	14.34	1.23	16	6 x 4	A row uniformly shaded
[30]		104.33	11.88	1.23	13	6 x 4	A column unevenly shaded
[30]		53.24	9.41	0.50	66	6 x 4	Random shading
[31]				3.1		9 x 9	A row uniformly shaded
[31]	//SM-TCT			3.55		9 x 9	A column unevenly shaded
[31]				3.58		9 x 9	Random shading
[31]				3.1		9 x 9	A row uniformly shaded
[31]	SM-TCT			3.48		9 x 9	A column unevenly shaded
[31]				3.81		9 x 9	Random shading
[31]				3.1		9 x 9	A row uniformly shaded
[31]	SM-TCT+BL			3.54		9 x 9	A column unevenly shaded
[31]				3.95		9 x 9	Random shading
[14]				4.2		9 x 9	Shading short and wide
[14]	Sudoku			5.3		9 x 9	Shading long and narrow
[14]				5.5		9 x 9	Shading short and narrow

All shading patterns reported are explained in detail in the Appendix.

Appendix A: Shading patterns

The following figures shows the shading patterns used in the performance description of the paper.

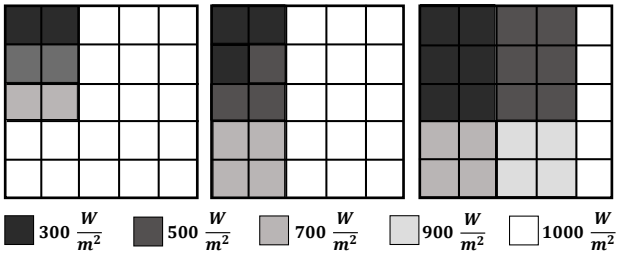

Figure 24. From right to left: 1) Short and narrow 2) Long and narrow 3) Long and wide [8].

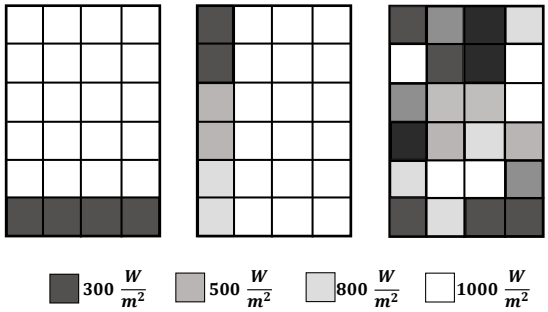

Figure 25. From right to left: 1) A row uniformly shaded 2) A column unevenly shaded 3) Random shading [25].

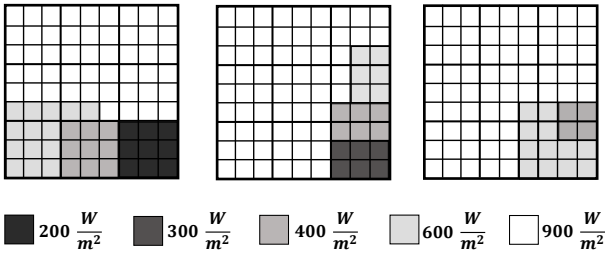

Figure 26. From right to left: 1) A column unevenly shaded 2) A row unevenly shaded 3) Random shading [11, 26].

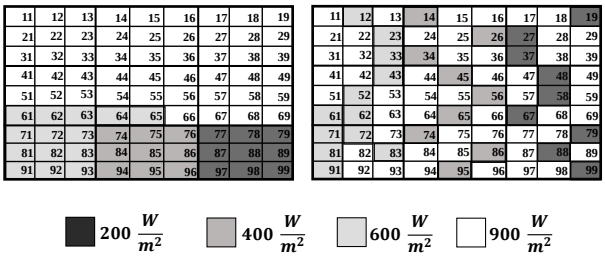

Figure 27. Shading pattern condition 1: shading dispersion using TCT arrangement (left) and Su Do Ku arrangement (right) [11].

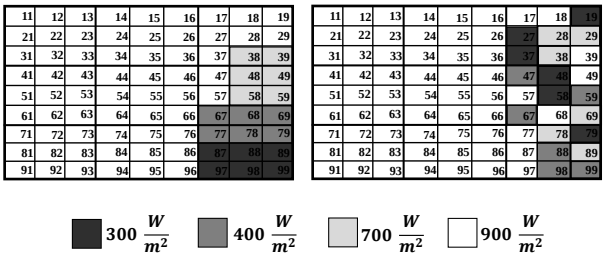

Figure 28. Shading pattern condition 2: shading dispersion using TCT arrangement (left) and Su Do Ku arrangement (right) [11].

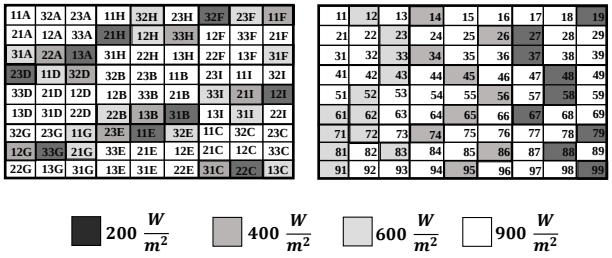

Figure 29. Shading pattern condition 1: shading dispersion using S-M-TCT arrangement (left) and Su Do Ku arrangement (right) [26].

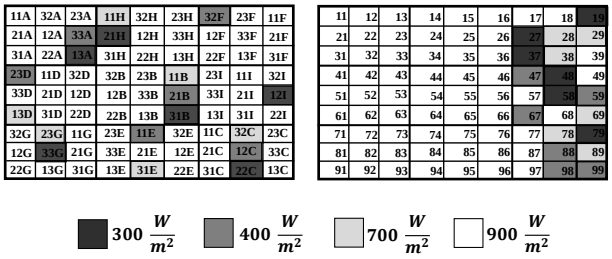

Figure 30. Shading pattern condition 1: shading dispersion using S-M-TCT arrangement (left) and Su Do Ku arrangement (right) [26].

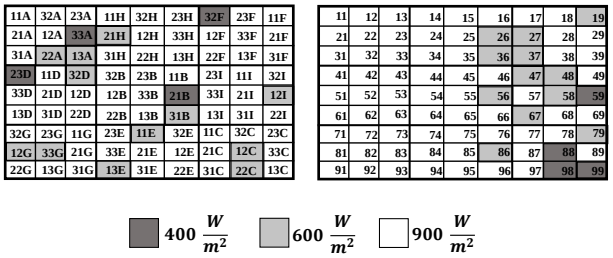

Figure 31. Shading pattern condition 1: shading dispersion using S-M-TCT arrangement (left) and Su Do Ku arrangement (right) [26].

References

1. Hariharan R, Chakkarapani M, Ilango GS, et al. (2016) A method to detect photovoltaic array faults and partial shading in PV systems. *IEEE J Photovoltaics* 6: 1278–1285.
2. Silvestre S, Kichou S, Chouder A, et al. (2015) Analysis of current and voltage indicators in grid connected pv (photovoltaic) systems working in faulty and partial shading conditions. *Energy* 86: 42–50.
3. Pendem SR, Mikkili S (2018) Modelling and performance assessment of pv array topologies under partial shading conditions to mitigate the mismatching power losses. *Sol Energy* 160: 303–321.
4. Ghanbari T (2017) Permanent partial shading detection for protection of photovoltaic panels against hot spotting. *IET Renew Power Gen* 11: 123–131.
5. Rossi D, Omana M, Giaffreda D, et al. (2015) Modeling and detection of hotspot in shaded photovoltaic cells. *IEEE T VLSI Syst* 23: 1031–1039.
6. Oliveri A, Cassottana L, Laudani A, et al. (2017) Two FPGA-oriented high-speed irradiance virtual sensors for photovoltaic plants. *IEEE T Ind Inform* 13: 157–165.
7. Carrasco M, Laudani A, Lozito GM, et al. (2017) Low-cost solar irradiance sensing for pv systems. *Energies* 10: 998.
8. Pendem SR, Mikkili S (2018) Modeling, simulation and performance analysis of solar pv array configurations (series, seriesparallel and honey-comb) to extract maximum power under partial shading conditions. *Sol Energy* 4: 274–287.
9. Hemalatha R, Ramaprabha R, Radha S (2015) A comprehensive analysis on sizing of solar energy harvester elements for wireless sensor motes. *Renew Sust Energ Rev* 8: 291–315.
10. El-Dein MZS, Kazerani M, Salama MMA (2012) Optimal total cross tied interconnection for photovoltaic arrays to reduce partial shading losses. In *Power and Energy Society General Meeting, IEEE*, 1–6.
11. Deshkar SN, Dhale SB, Mukherjee JS, et al. (2015) Solar pv array reconfiguration under partial shading conditions for maximum power extraction using genetic algorithm. *Renew Sust Energ Rev* 43: 102–110.

12. Mohanty S, Subudhi B, Ray PK (2016) A new mppt design using grey wolf optimization technique for photovoltaic system under partial shading conditions. *IEEE T Sustain Energ* 7: 181–188.

13. Mahmoud Y, El-Saadany EF (2016) Fast power-peaks estimator for partially shaded PV systems. *IEEE T Energy Conver* 31: 206–217.

14. Celik B, Karatepe E, Silvestre S, et al. (2015) Analysis of spatial fixed pv arrays configurations to maximize energy harvesting in bipv applications. *Renew Energ* 75: 534–540.

15. Cristaldi L, Faifer M, Rossi M, et al. (2014) Simplified method for evaluating the effects of dust and aging on photovoltaic panels. *Measurement* 54: 207–214.

16. Faba A, Gaiotto S, Lozito GM (2017) A novel technique for online monitoring of photovoltaic devices degradation. *Sol Energy* 158: 520–527.

17. Bai J, Cao Y, Hao Y, et al. (2015) Characteristic output of pv systems under partial shading or mismatch conditions. *Sol Energy* 112: 41–54.

18. Ahmed J, Salam Z (2015) A critical evaluation on maximum power point tracking methods for partial shading in pv systems. *Renew Sust Energ Rev* 47: 933–953.

19. Kofinas P, Dounis AI, Papadakis G, et al. (2015) An intelligent mppt controller based on direct neural control for partially shaded pv system. *Energ Buildings* 90: 51–64.

20. Kotti R, Shireen W (2015) Efficient mppt control for pv systems adaptive to fast changing irradiation and partial shading conditions. *Sol Energy* 114: 397–407.

21. Sundareswaran K, Vignesh kumar V, Palani S (2015) Application of a combined particle swarm optimization and perturb and observe method for mppt in pv systems under partial shading conditions. *Renew Energ* 75: 308–317.

22. Benyoucef AS, Chouder A, Kara K, et al. (2015) Artificial bee colony based algorithm for maximum power point tracking (mppt) for pv systems operating under partial shaded conditions. *Appl Soft Comput* 32: 38–48.

23. Laudani A, Fulginei FR, Salvini A, et al. (2014) Implementation of a neural mppt algorithm on a low-cost 8-bit microcontroller. In *Power Electronics, Electrical Drives, Automation and Motion (SPEEDAM), 2014 International Symposium on, IEEE*, 977–981.

24. Lozito GM, Bozzoli L, Salvini A (2014) Microcontroller based maximum power point tracking through fcc and mlp neural networks. In *Education and Research Conference (EDERC), 2014 6th European Embedded Design in*, 207–211.

25. Belhachat F, Larbes C (2015) Modeling, analysis and comparison of solar photovoltaic array configurations under partial shading conditions. *Sol Energy* 120: 399–418.

26. Belhaouas N, Cheikh MSA, Agathoklis P, et al. (2017) Pv array power output maximization under partial shading using new shifted pv array arrangements. *Appl Energ* 187: 326–337.

27. Bastidas-Rodrgueza JD, Trejos-Grisalesb LA, Gonzlez-Montoyac D, et al. (2018) General modeling procedure for photovoltaic arrays. *Electr Pow Syst Res*. 155: 67–79.

28. Gonzlez-Montoyac D, Bastidas-Rodrgueza JD, Trejos-Grisalesb LA, et al. (2018) A procedure for modeling photovoltaic arrays under any configuration and shading conditions. *Energies* 11: 767.

29. Babu TS, Ram JP, Dragievi T, et al. (2018) Particle swarm optimization based solar PV array reconfiguration of the maximum power extraction under partial shading conditions. *IEEE T Sustain Energ* 9: 74–85.

30. Ram JP, Rajasekar N (2017) A novel flower pollination based global maximum power point method for solar maximum power point tracking. *IEEE T Power Electr* 32: 8486–8499.

31. Iraji F, Farjah E, Ghanbari T (2018) Optimisation method to find the best switch set topology for reconfiguration of photovoltaic panels. *IET Renew Power Gen* 12: 374–379.

32. Dhimish M, Holmes V, Mehrdadi B, et al. (2017) Seven indicators variations for multiple pv array configurations under partial shading and faulty pv conditions. *Renew Energ* 113: 438–460.

33. Potnuru SR, Pattabiraman D, Ganesan SI, et al. (2015) Positioning of pv panels for reduction in line losses and mismatch losses in pv array. *Renew Energ* 78: 264–275.

34. Vijayalekshmy S, Bindu GR, Iyer SR (2016) A novel zig-zag scheme for power enhancement of partially shaded solar arrays. *Sol Energy* 135: 92–102.

35. Dhanalakshmi B, Rajasekar N (2018) Dominance square based array reconfiguration scheme for power loss reduction in solar photovoltaic (pv) systems. *Energ Convers Manage* 156: 84–102.

36. Rezaii R, Ameri MH, Varjani AY, et al. (2018) Overcoming partial shading issue of pv modules by using a resonant switched capacitor converter. In *Power Electronics, Drives Systems and Technologies Conference (PEDSTC), 2018 9th Annual*, 38–43.

37. Uno M, Kukita A (2015) Single-switch voltage equalizer using multistacked buck–boost converters for partially shaded photovoltaic modules. *IEEE T Power Electr* 30: 3091–3105.

38. Chub A, Vinnikov D, Kosenko R, et al. (2017) Wide input voltage range photovoltaic microconverter with reconfigurable buck–boost switching stage. *IEEE T Ind Electron* 64: 5974–5983.

39. Vinnikov D, Chub A, Roasto I, et al. (2016) Multi-mode quasi-z-source series resonant DC/dc converter for wide input voltage range applications. In *Applied Power Electronics Conference and Exposition (APEC),IEEE*, 2533–2539.

40. Ikkurti HP, Saha S (2015) A comprehensive techno-economic review of microinverters for building integrated photovoltaics (bipv). *Renew Sust Energ Rev* 47: 997–1006.

41. Hasan R, Mekhilef S (2017) Highly efficient flyback microinverter for grid-connected rooftop pv system. *Sol Energy* 146: 511–522.

42. Uno M, Kukita A (2013) Two-switch voltage equalizer using series-resonant inverter and voltage multiplier for partially-shaded series-connected photovoltaic modules. In *Energy Conversion Congress and Exposition, IEEE*.

43. Famoso F, Lanzafame R, Maenza S, et al. (2015) Performance comparison between micro-inverter and string-inverter photovoltaic systems. *Energy Procedia* 81: 526–539.

44. Bauwens P, Doutreloigne J (2014) Reducing partial shading power loss with an integrated smart bypass. *Sol Energy* 103: 134–142.

45. Daliento S, Di Napoli F, Guerriero P, et al. (2016) A modified bypass circuit for improved hot spot reliability of solar panels subject to partial shading. *Sol Energy* 134: 211–218.

46. Kim KA, Krein PT (2015) Reexamination of photovoltaic hot spotting to show inadequacy of the bypass diode. *IEEE J Photovolt* 5: 1435–1441.

47. Dhimish M, Holmes V, Mehrdadi B, et al. (2018) Output-power enhancement for hot spotted polycrystalline photovoltaic solar cells. *IEEE T Device Mat Re* 18: 37–45.

48. Winston DP, Kumar BP, Christabel SC, et al. (2018) Maximum power extraction in solar renewable power system - a bypass diode scanning approach. *Comput Electr Eng*.

49. Daliento S, Chouder A, Guerriero P, et al. (2017) Monitoring, diagnosis, and power forecasting for photovoltaic fields: A review. *Int J Photoenergy* 2017: 1–13.

50. Mellit A, Tina GM, and Kalogirou SA (2018) Fault detection and diagnosis methods for photovoltaic systems: A review. *Renew Sust Energ Rev* 91: 1–17.

51. Ali MH, Rabhi A, Hajjaji AE, et al. (2017) Real time fault detection in photovoltaic systems. *Energy Procedia* 111: 914–923.

52. Laudani A, Fulginei FR, Salvini A (2014) High performing extraction procedure for the one-diode model of a photovoltaic panel from experimental iv curves by using reduced forms. *Sol Energy* 103: 316–326.

53. Laudani A, Fulginei FR, and Salvini A (2014) Identification of the one-diode model for photovoltaic modules from datasheet values. *Sol Energy* 108: 432–446.

54. Laudani A, Fulginei FR, Salvini A, et al. (2014) Very fast and accurate procedure for the characterization of photovoltaic panels from datasheet information. *Int J Photoenergy*.

55. Silvestre S, da Silva MA, Chouder A, et al. (2014) New procedure for fault detection in grid connected pv systems based on the evaluation of current and voltage indicators. *Energ Convers Manage* 86: 241–249.

56. Mahendran M, Anandharaj V, Vijayavel K, et al. (2015) Permanent mismatch fault identification of photovoltaic cells using arduino. *ICTACT J MICROELECTRON* 01: 79–82.

57. Stauffer Y, Ferrario D, Onillon E, et al. (2015) Power monitoring based photovoltaic installation fault detection. In *2015 International Conference on Renewable Energy Research and Applications (ICRERA)*.

58. Mekki H, Mellit A, Salhi A (2016) Artificial neural network-based modelling and fault detection of partial shaded photovoltaic modules. *Simul Model Pract Th* 67: 1–13.

59. Garoudja E, Chouder A, Kara K, et al. (2017) An enhanced machine learning based approach for failures detection and diagnosis of pv systems. *Energ Convers Manage* 151: 496–513.

60. Belaout A, Krim F, Mellit A (2016) Neuro-fuzzy classifier for fault detection and classification in photovoltaic module. In *Proc. Identification and Control (ICMIC) 2016 8th Int. Conf. Modelling*, 144–149.

61. Dhimish M, Holmes V, Mehrdadi B, et al. (2017) Photovoltaic fault detection algorithm based on theoretical curves modelling and fuzzy classification system. *Energy* 140: 276–290.

62. Tsanakas JA, Ha LD, Al Shakarchi F (2017) Advanced inspection of photovoltaic installations by aerial triangulation and terrestrial georeferencing of thermal/visual imagery. *Renew Energ* 102:224–233.

63. Tsanakas JA, Ha L, Buerhop C (2016) Faults and infrared thermographic diagnosis in operating c-si photovoltaic modules: A review of research and future challenges. *Renew Sust Energ Rev* 62: 695–709.

64. Zorn C, Kaminski N (2015) Acceleration of temperature humidity bias (thb) testing on igbt modules by high bias levels. In *2015 IEEE 27th International Symposium on Power Semiconductor Devices & IC's (ISPSD)*.

65. Laudani A, Lozito GM, Lucaferri V, et al. (2017) An analytical approach for maximum power point calculation for photovoltaic system. In *Circuit Theory and Design (ECCTD), 2017 European Conference on*, 1–4.

AIMS Press